JOURNAL OF SOLID STATE CHEMISTRY 98, 105–120 (1992)

Structural and Optical Properties of Calcium Neodymium Hexaaluminates Single Crystals, Potential Laser Materials

S. ALABLANCHE,*,† A. KAHN-HARARI,* J. THERY,*,‡ B. VIANA,* AND D. VIVIEN*

Laboratoire de Chimie Appliquée de l'Etat Solide, CNRS URA 1466, ENSCP, 11 rue P. et M. Curie, 75231 Paris Cedex 05, France; and †Quartz et Silice, 108 avenue Carnot, 77793 Nemours Cedex, France

AND J. DEXPERT-GHYS AND M. FAUCHER

Laboratoire des Eléments de Transition dans les Solides, CNRS-ER 60210, 1 Place A. Briand, 92195 Meudon Cedex, France

Received July 25, 1991; in revised form October 28, 1991

The structural and optical properties of calcium–neodymium hexaaluminates crystals $Ca_{1-x}Nd_xMg_xAl_{12-x}O_{19}$ (labeled $Ca_{1-x}Nd_x$) with a magnetoplumbite (MP) structure are investigated. The floating zone method is used to grow single crystals in the composition range $0.1 \leq x \leq 0.7$, although for high calcium content, the melting of the compounds is no longer congruent. The X-ray structural determination, optical absorption at 4 K, and ESR investigation agree in the localization of Nd^{3+} at the regular large cations site of the MP structure with axial (D_{3h}) symmetry. A set of crystal field and free ion parameters which fits the absorption spectrum of Nd^{3+} in this site is calculated. When x increases, Nd^{3+} ions tend to occupy also a second site with lower symmetry. Moreover some anomalous behavior observed in the absorption and ESR spectra at high neodymium concentration may be related to Nd^{3+}–Nd^{3+} ion pairing. Fluorescence intensity and lifetime measurements as a function of the x value are reported. There is evidence of strong cross-relaxation between neighboring neodymium ions for high x values. The results obtained for the $Ca_{1-x}Nd_x$ compounds can be extended to other series in which Nd^{3+} is replaced by another lanthanide ion. Preliminary investigations have been performed with Pr^{3+} and are also reported.

Introduction

The calcium ($CaAl_{12}O_{19}$) and lanthanide ($LnMgAl_{11}O_{19}$ with $Ln = La_{1-\alpha}Nd_\alpha$) hexaaluminates form a full series of solid solutions (labeled CLnA) of the magnetoplumbite (MP) type (*1*). Single crystals have already been grown by the zone melting technique, using an arc image furnace, for various starting compositions $Ca_{1-x}Ln_xMg_xAl_{12-x}O_{19}$ with $Ln = La_{1-\alpha}Nd_\alpha$, $0 \leq \alpha \leq 1$ and $0.3 \leq x \leq 0.7$. Optical absorption, fluorescence, and ESR spectra of Nd^{3+} in these mixed crystals have been investigated and compared with those of $La_{1-x}Nd_xMgAl_{11}O_{19}$ (LNA) which is a promising laser material (*2, 3*). In LNA, Nd^{3+} ions are distributed on three sites, whereas in CLnA only two of these sites were shown to be occupied (*1*). Furthermore, one of the two sites, with

‡ To whom correspondence should be addressed.

0022-4596/92 $5.00

nearly axial symmetry, is much more populated than the other. The higher the calcium content of C*Ln*A, the higher the neodymium occupancy ratio in this axial site (*1*). Therefore, a comprehensive study of C*Ln*A compounds for $Ln = Nd^{3+}$ (referred to as $Ca_{1-x}Nd_x$) is reported here, particularly in the calcium-rich composition range $0.1 \leq x \leq 0.7$. We have also been interested in the effect of neodymium dilution which is thought necessary to prevent concentration quenching of the fluorescence. It could be achieved either by varying the calcium content of the material or by introducing another lanthanide ion such as lanthanum.

Crystals of every chosen composition are elaborated by floating zone method. Characterization of the magnetoplumbite structure is made by X-ray powder diffraction. Two crystalline compositions were selected for intensity measurements and structure refinement. The more specific study of the Nd^{3+} ion (site number and symmetry) is realized by ESR and optical absorption spectroscopies, and calculation of the crystal field parameters. The optical behavior of these compounds is tested with regard to their possible laser application (fluorescence intensity and lifetime).

Experimental

At first for every composition $Ca_{1-x}Nd_x$ or $Ca_{1-x}(La_{1-y}Nd_y)$ with $0 < y < 1$ and $0.1 \leq x \leq 0.7$, sintered rungs are prepared in the following way: $CaCO_3$, La_2O_3, Nd_2O_3, Al_2O_3, and MgO powders are mixed in the appropriate amounts. The intimate mixture is cold pressed and the pellets are prereacted by heating at 1100°C in air for 15 hr in order to decompose the carbonates. The samples are crushed, pressed again to obtain parallelepipedic rungs (5 cm in length, 1 cm in width), and then annealed for 50 hr at 1560°C. X-ray powder diffraction is used to check that the reaction is completed. Rungs are shaped into rods to be used in the crystal growth by the floating zone method in air. The heat source is a focused 6.5-kW xenon arc lamp. Every composition is processed with a 1 cm/hr translation speed. The crystalline quality is related to the calcium concentration and decreases when this concentration increases.

The growth of the $Ca_{0.5}Nd_{0.5}$ (or $Ca_{0.5}La_{0.4}Nd_{0.1}$) and $Ca_{0.6}Nd_{0.4}$ compounds provide transparent crystals (5 mm in diameter, 5 cm in length) with the MP structure. They exhibit a few cracks, probably due to thermal shock under cooling. The compounds with higher calcium concentration show not only cracks but also extra phases. The $Ca_{0.8}Nd_{0.2}$ (and $Ca_{0.8}La_{0.1}Nd_{0.1}$) crystal is of quite a good quality but uniformly covered with a thin white polycrystalline layer of a αAl_2O_3–$CaAl_4O_7$ mixture. In the case of $Ca_{0.9}Nd_{0.1}$, under the polycrystalline layer, we only find a few monocrystalline platelets of the MP phase mixed with alumina. The occurrence of parasitic phases may arise from the noncongruent melting for these compositions, as it occurs for the parent compound $CaAl_{12}O_{19}$.

The crystal growth always occurs along the **a** axis. By mechanical shock, the crystal can be cleaved along the (**a, b**) plane leading to monocrystalline slabs suitable for spectroscopic or structural investigations. The exact compositions in Ca^{2+}, Nd^{3+}, Mg^{2+}, and Al^{3+} are determined by electron probe microanalysis. Experimental compositions and lattice parameters are given in Table I. After the crystal growth process, we observe a lack of calcium with regard to the starting compositions. The microprobe analysis along the crystal length indicates that there is no segregation of the elements.

The effect of magnesium is also pointed out. An excess or a deficiency of MgO in the starting mixture, balanced or not by the Al_2O_3 content, always leads to platelets of MP crystals and simultaneous formation of other phases.

TABLE I

CHEMICAL COMPOSITIONS AND LATTICE PARAMETERS OF *CLnA* SINGLE CRYSTALS AND THE LNA COMPOUND

Starting compositions	Formulas deduced from electron probe microanalysis	Lattice parameters (powder patterns)	
		a (±0.002) (Å)	c (±0.005) (Å)
$Ca_{0.9}Nd_{0.1}$	$Ca_{0.847}Nd_{0.139}Mg_{0.120}Al_{11.882}O_{19}$	5.562	21.89
$Ca_{0.8}La_{0.1}Nd_{0.1}$	$Ca_{0.691}La_{0.133}Nd_{0.142}Mg_{0.257}Al_{11.757}O_{19}$	5.565	21.91
$Ca_{0.8}Nd_{0.2}$	$Ca_{0.743}Nd_{0.252}Mg_{0.232}Al_{11.765}O_{19}$	5.565	21.89
$Ca_{0.7}Nd_{0.3}$	$Ca_{0.630}Nd_{0.320}Mg_{0.270}Al_{11.700}O_{19}$	5.570	21.89
$Ca_{0.6}Nd_{0.4}$	$Ca_{0.474}Nd_{0.490}Mg_{0.414}Al_{11.558}O_{19}$	5.568	21.89
$Ca_{0.5}La_{0.4}Nd_{0.1}$	$Ca_{0.441}La_{0.479}Nd_{0.063}Mg_{0.463}Al_{11.519}O_{19}$	5.574	21.94
$Ca_{0.5}Nd_{0.5}$	$Ca_{0.404}Nd_{0.575}Mg_{0.443}Al_{11.506}O_{19}$	5.577	21.90
$Ca_{0.4}Nd_{0.6}$	$Ca_{0.332}Nd_{0.581}Mg_{0.491}Al_{11.536}O_{19}$	5.571	21.88
LNA[a]		5.579	21.97

[a] Data from Ref. (*4*).

X-Ray Structural Investigation

Compounds belonging to the magnetoplumbite structure type have a hexagonal symmetry with space group $P6_3/mmc$. The corresponding unit cell contains two unit formulas and consists in two spinel-like blocks "$Al_{11}O_{16}$," separated by mirror planes containing the heavy ions, three oxygen ions, and one more Al ion (Fig. 1), (*4*). This ideal structure has been found to accommodate a wide range of disorder and nonstoichiometry. In $CaAl_{12}O_{19}$ for instance, substitution of Ln^{3+} to some Ca^{2+} requires some electric compensation, such as Mg^{2+} substitution for Al^{3+}, in the spinel blocks. In materials exhibiting different Ca^{2+}/Nd^{3+} ratios, the main need is to determine the exact location of these ions with respect to the possible positions of $P6_3/mmc$ on which they are expected to lie.

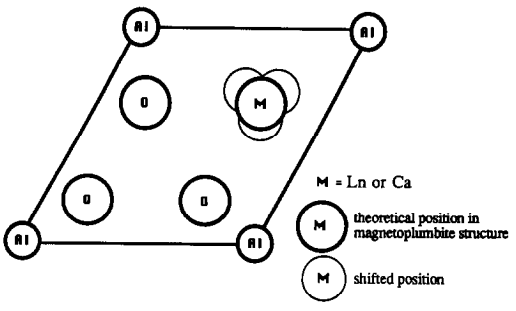

FIG. 1. Mirror plane structure in magnetoplumbite.

Two crystals were selected for intensity measurements and structure refinement, respectively, with $Ca_{0.8}Nd_{0.2}$ and $Ca_{0.5}Nd_{0.5}$ starting compositions, in order to determine the exact location and environment of the Nd^{3+} active ion in these materials. Refinement of both structures was performed (*5*, *6*) on two sets of intensities collected on a CAD4 Nonius diffractometer. The specific parameters of the crystals and conditions of data collection are gathered in Table II. The resulting atomic parameters for each compound and corresponding interatomic distances are given in Tables III, IV, and V.

In both refined structures, Ca and Nd are undiscernable. Attempts were made to localize them independently, but with both compositions they have to be handled as an average weighted ion such as 0.8Ca + 0.2Nd and 0.5Ca + 0.5Nd. Their exact location as deduced from refined atomic positions and occupancy is on the ideal 2*d*

TABLE II

CRYSTALLOGRAPHIC DATA AND PROCEDURE

$Ca_{0.8}Nd_{0.2}(Al,Mg)_{12}O_{19}$ magnetoplumbite	$Ca_{0.5}Nd_{0.5}(Al,Mg)_{12}O_{19}$
Crystal symmetry Hexagonal	Crystal symmetry Hexagonal
Space group $P6_3/mmc$ $Z = 2$	Space group $P6_3/mmc$ $Z = 2$
Unit cell $a = b = 5.558$ (±0.001) Å	Unit cell $a = b = 5.568$ (±0.001) Å
$c = 21.872$ (±0.002) Å $\gamma = 120°$	$c = 21.883$ (±0.004) Å $\gamma = 120°$
$c/a = 3.935$ $V = 585$ Å^3	$c/a = 3.93$ $V = 588$ Å^3
Density $\rho th = 3.98$	Density $\rho th = 4.10$
Crystal size $0.3 \times 0.4 \times 0.17$ mm	Crystal size $0.2 \times 0.3 \times 0.05$ mm
Linear absorption coefficient $\mu = 81$ cm^{-1}	Linear absorption coefficient $\mu = 90$ cm^{-1}
Data collection Nonius CAD4 diffractometer	
λMo$K\alpha$, 0.7107 Å; graphite monochromator; θ/ω scan, scanning speed: 1.5° to 6.7°/min	
$0 < h < 8, 0 < k < 8, 0 < l < 40$	$0 < h < 10, 0 < k < 10, 0 < l < 40$
$\sin \theta/\lambda_{max} = 0.95$	$\sin \theta/\lambda_{max} = 0.95$
Total of measured reflections: 1265 independent of which 192 unobserved with $I < 3\sigma$	Total of measured reflections: 1241 independent, of which 359 unobserved with $I < 3\ \sigma$
Ion scattering factors from International Tables for X-Ray Crystallography, Vol. IV	
R factor on $\lvert F(hkl)\rvert$ 0.029	R factor on $\lvert F(hkl)\rvert$ 0.032
Weighted R: 0.032	Weighted R: 0.037
544 reflections ($F > F_{max}/20$)	501 independent reflections ($F > F_{max}/20$)
One average Ca/Nd site	Two partially occupied Ca/Nd sites
Residual electron density: 0.9 e/Å^3	Residual electron density: 1.2 e/Å^3
Extinction correction factor: 0.32×10^{-5}	Extinction correction factor: 0.22×10^{-5}

Wyckoff position ($\frac{2}{3}$, $\frac{1}{3}$, $\frac{1}{4}$) or quite close to it (6*h* position). Of course, this is an average description, meaning that in any considered unit cell, the (Ca/Nd) ion is found on only one of the four possible sites shown in Fig. 1. The environment around the 2*d* position is more symmetrical (D_{3h}) than the 6*h* shifted one (C_{2v}). For the $Ca_{0.8}Nd_{0.2}$ composition, the mean ion can be taken in the 2*d* site with a corresponding thermal factor B of 0.4; however, anisotropic refinement of temperature factors shows that this ion exhibits a large amplitude of vibration within the mirror plane. Handling the average weighted ion of the $Ca_{0.5}Nd_{0.5}$ composition in the same way leads to a bad R factor and too large amplitudes of vibration. Therefore, this ion is also introduced on a second slightly shifted position; then the thermal factors have more reasonable values for both partly occupied sites. It comes out that the higher the Nd^{3+} content, the more disordered the distribution of heavy ions in the mirror planes of the structure. As previously mentioned in similar compounds (*7*), the A12 ion, theoretically located at the 2*b* position, is shifted out of the mirror plane, locally disturbing its fivefold oxygen environment to get into a tetrahedral site.

ESR Investigations of Nd^{3+} in $Ca_{1-x}Nd_x$

The ESR spectra of single crystals of the $Ca_{1-x}Nd_x$ compounds were obtained at 20 K on a Bruker ER 220 D spectrometer operating at the X band, fitted with an Oxford Instrument ESR 9 helium flow cryostat. The crystalline slabs are parallel to the (**a, b**) plane of the structure. The spectra were performed for different orientations of the static

TABLE III

FINAL SET OF ATOMIC PARAMETERS IN $Ca_{0.8}Nd_{0.2}$ HEXAALUMINATE (R = 0.029)

Atom type	Wyckoff position	No. of neighbors	Coordinates			Isotropic thermal B coefficient
			x	$y = 2x$	z	
Al1	2*a*	6	0.	0.	0.	0.10(3)
Al2	2*b*	4 + 1	0.	0.	0.2411(1)	0.16(5)
Al3 (Al + Mg)	4*f*	4	0.3334	0.6667	0.0277(1)	0.23(2)
Al4	4*f*	6	0.3334	0.6667	0.1906(1)	0.18(2)
Al5	12*k*	6	−0.1682(1)	−0.3365	0.1089(0)	0.19(1)
O1	4*e*		0.	0.	0.1497(1)	0.27(5)
O2	4*f*		0.6667	0.3334	0.0557(1)	0.31(5)
O3	6*h*		0.1812(3)	0.3623	0.250	0.51(4)
O4	12*k*		0.1543(2)	0.3086	0.0526(1)	0.33(3)
O5	12*k*		0.5040(3)	0.0079	0.1499(1)	0.29(3)
Ca/Nd	6*h*	12	0.6736(6)	0.3472	0.250	0.40(5)

Note. Estimated standard deviations are given in parentheses. Coordinates without e.s.d. are unvariable.

magnetic field B_0 with respect to the **c** axis of the crystals.

$B_0 \parallel$ **c**. For this orientation, the lines are the narrowest, the intensities are maxima, and the field positions are minima. This indicates that **c** is one of the principal axes of the g tensor of Nd^{3+} ions. As seen in Fig. 2, the spectra are always constituted of a narrow central line (associated with Nd^{3+} ions of zero nuclear spin) which corresponds to a single type of site occupied by neodymium. On the contrary, in the LNA case, there are two central lines (*8*) which reveal the multisite character of the neodymium ions. This central line is flanked by weak hyperfine satellites due to

TABLE IV

FINAL SET OF ATOMIC PARAMETERS IN $Ca_{0.5}Nd_{0.5}$ HEXAALUMINATE (R = 0.032)

Atom type	Wyckoff position	No. of neighbors	Coordinates			Isotropic thermal B coefficient
			x	$y = 2x$	z	
Al1	2*a*	6	0.	0.	0.	0.24(4)
Al2	2*b*	4 + 1	0.	0.	0.2416(1)	0.35(6)
Al3 (Al + Mg)	4*f*	4	0.3334	0.6667	0.0276(1)	0.30(3)
Al4	4*f*	6	0.3334	0.6667	0.1903(1)	0.20(2)
Al5	12*k*	6	−0.1680(1)	−0.3361	0.1087(0)	0.23(1)
O1	4*e*		0.	0.	0.1499(4)	0.43(6)
O2	4*f*		0.6667	0.3334	0.0566(4)	0.38(5)
O3	6*h*		0.1810(3)	0.3621	0.250	0.54(5)
O4	12*k*		0.1533(2)	0.3067	0.0529(1)	0.40(3)
O5	12*k*		0.5048(3)	0.0096	0.1508(1)	0.30(3)
Ca/Nd (0.6/plane)	2*d*	12	0.6667	0.3334	0.250	0.30(5)
Ca/Nd (0.4/plane)	6*h*	12	0.6855(4)	0.3708	0.250	0.40(5)

Note. Estimated standard deviations are given in parentheses. Coordinates without e.s.d. are unvariable.

TABLE V

INTERATOMIC BOND LENGTHS IN $Ca_{1-x}Nd_x$ HEXAALUMINATES (IN Å)

Hexaaluminate $Ca_{0.5}Nd_{0.5}$ (R = 0.032)			Hexaaluminate $Ca_{0.8}Nd_{0.2}$ (R = 0.028)		
NdCa1–O5	×6	2.673(2)			
(2*d*) O3	×6	2.787(3)			
NdCa2–O5	×4	2.626(2)	NdCa– O5	×4	2.673(3)
(6*h*) O3	×2	2.636(4)	(6*h*) O3	×2	2.726(3)
O5	×2	2.783(2)	O5	×2	2.731(2)
O3	×2	2.784(4)	O3	×2	2.780(4)
O3	×2	2.950(4)	O3	×2	2.842(4)
Al1–O4	×6	1.878(2)	Al1–O4	×6	1.879(1)
(2*a*)					
Al2–O3	×3	1.756(2)	Al2–O3	×3	1.755(1)
(2*b*) O1		2.006(9)	O1		1.997(3)
O1		*2.374(9)*	*O1*		*2.391(3)*
Al3–O4	×3	1.822(2)	Al3–O4	×3	1.808(1)
(4*f*) O2		1.842(9)	O2		1.824(3)
Al4–O5	×3	1.866(2)	Al4–O5	×3	1.869(2)
(4*f*) O3	×3	1.966(2)	O3	×3	1.958(2)
Al5–O5	×2	1.826(2)	Al5–O5	×2	1.814(2)
(12*k*) O1		1.856(4)	O1		1.849(1)
O2	×2	1.958(5)	O2	×2	1.970(2)
O4		1.978(2)	O4		1.985(2)

Note. The e.s.d. is in parentheses.

the two neodymium isotopes, both with 7/2 nuclear spin, and by two lines whose intensity greatly increases with the Nd^{3+} concentration (Fig. 2). Similar phenomena have been observed in other compounds and attributed to Nd^{3+} pairs (*9*). Here too, these lines may reveal the existence of magnetic interactions between the Nd^{3+} ions.

When the magnetic field rotates from the **c** axis to the direction of the (**a, b**) plane, the lines move towards higher fields and broaden. For B_0 perpendicular to the **c** axis the lines reach their higher field positions.

$B_0 \perp$ **c**. When B_0 rotates into the (**a, b**) plane, the ESR spectrum is mainly constituted of a broad line, nearly isotropic. However, its position exhibits a very small fluctuation with a 60° periodicity. This indicates that the main site for the Nd^{3+} ion in the $Ca_{1-x}Nd_x$ compounds is not perfectly axial, even for very low x values, but is very close to the theoretical (2*d*) large cation site of the magnetoplumbite structure with D_{3h} symmetry.

Optical Absorption of Nd^{3+}

The spectra were recorded at 4 K on a Beckmann UV 5270 spectrometer fitted with an Oxford Instrument helium flow cryostat, in the wavelength range 200 to 2600 nm. The light beam was directed along the crystal **c** axis. The number of absorption lines detected in the $^4I_{9/2} \rightarrow {}^2P_{1/2}$ region (420–440 nm) at liquid helium

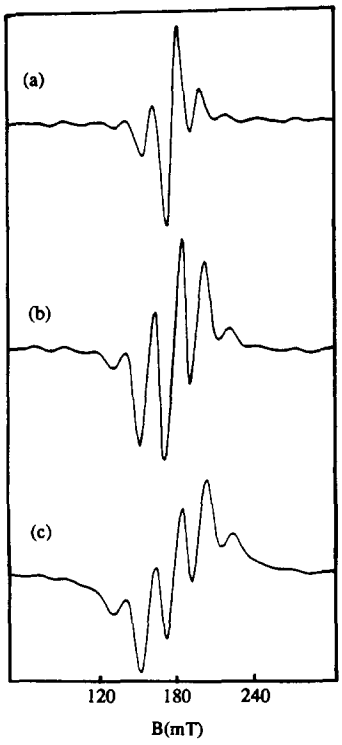

FIG. 2. Comparison of the single-crystal ESR spectra with $B_0 /\!/ \mathbf{c}$ of Nd^{3+} for three *CLnA* compounds with starting compositions: (a) $Ca_{0.9}Nd_{0.1}$; (b) $Ca_{0.8}Nd_{0.2}$; and (c) $Ca_{0.7}Nd_{0.3}$.

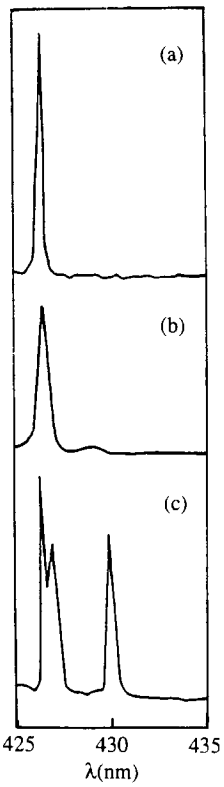

FIG. 3. Influence of the Ca/*Ln* ratio on the optical absorption spectrum of the Nd^{3+} $^4I_{9/2} \rightarrow {}^2P_{1/2}$ transition at 4 K. Starting compositions: (a) $Ca_{0.8}Nd_{0.2}$; (b) $Ca_{0.7}Nd_{0.3}$; and (c) LNA.

temperature can be used to determine the number of Nd^{3+} sites in a given structure. The terminating level $^2P_{1/2}$ is not split by the crystal field ($J + \frac{1}{2} = 1$). At sufficiently low temperature, the first Stark level of the $^4I_{9/2}$ ground state is the only one to be populated. Therefore, this transition gives a single line for each Nd^{3+} site. For LNA, the neodymium is distributed on three sites (*8*). As shown on Fig. 3c, two of them (giving a doublet at 426.2 and 426.6 nm) are very similar and the third one is responsible for the line peaking at 429.7 nm. In a parallel study by Agladze *et al.* (*10*) only two sites ($^2P_{1/2}$ = 426.7 and 429.9 nm at 77 K), but with broad absorption lines, were identified. In the C*Ln*A case, it has been shown that neodymium ions tend to become localized on a single site when the calcium concentration increases (*1*). The 428.7 nm line of the second site, corresponding to the 429.7 nm line in LNA, disappears (Fig. 3b).

The present work extends these results to compositions with higher calcium content: $Ca_{0.8}Nd_{0.2}$ and $Ca_{0.9}Nd_{0.1}$. In both cases, there is only one narrow line around 426.6 nm for the $^4I_{9/2} \rightarrow {}^2P_{1/2}$ transition at 4 K and therefore a single neodymium site. (Fig. 3a). Compared to LNA, the lines at higher wavelengths in a given transition tend to disappear: for instance the lines up to 581 nm in the hypersensitive transition $^4I_{9/2} \rightarrow {}^4G_{5/2}$, $^4G_{7/2}$, and $^2G_{7/2}$.

The optical absorption measurements at low temperature also indicate that the crystal field splitting of the energy levels is related to the calcium content in the matrix. The splitting usually decreases when the calcium concentration increases. The splitting of the $^4F_{3/2}$ level also follows this general rule (Fig. 4). But its precise value is difficult to estimate because of the occurrence of more than the two expected bands at 4 K, even at very high calcium concentration (Fig. 4a). This observation is also in disagreement with the single site character already established for these compositions by the X-ray diffraction and ESR investigations, and confirmed by the study of the $^4I_{9/2} \rightarrow {}^2P_{1/2}$ transition.

The key role of magnesium in C*Ln*A is confirmed by optical absorption spectroscopy. Investigation indicates that the second site occupancy (line around 428.7 nm) increases when the magnesium concentration decreases.

Analysis and Simulation of the Absorption Spectra

Well-isolated transitions observed in the absorption spectra at 4 K are easily attrib-

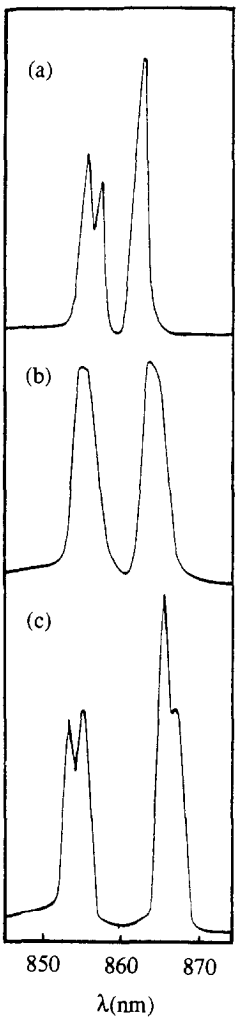

FIG. 4. Comparison of the optical absorption spectra of the Nd^{3+} $^4I_{9/2} \rightarrow {}^4F_{3/2}$ transition at 4 K. Starting compositions: (a) $Ca_{0.8}Nd_{0.2}$; (b) $Ca_{0.5}Nd_{0.5}$; and (c) LNA.

uted by reference to previous investigations on Nd^{3+} in other matrixes (*8*, *11–13*). The upper components of the ground state level are deduced by comparing the $^4F_{3/2} \rightarrow {}^4I_{9/2}$ emission spectra and the $^4I_{9/2} \rightarrow {}^2P_{1/2}$ absorption lines at room temperature. Ninety-five levels are identified for $Ca_{0.8}Nd_{0.2}$ (Table VI). Most of the observed transitions up to 29,000 cm^{-1} present a number of lines equal to or lower than the theoretical one, with the unique exception of $^4I_{9/2} \rightarrow {}^4F_{3/2}$. In the UV region (above 29,000 cm^{-1}) only a few lines could be detected. Three lines are observed in the $^4I_{9/2} \rightarrow {}^4F_{3/2}$ region, a very intense one is observed at 11,596 cm^{-1}, and a doublet is observed at 11,662 and 11,685 cm^{-1} (Fig. 4a). Up to now, we have no explanation for the occurrence of a supplementary line. We selected the couple (11,596–11,662 cm^{-1}) as discussed below.

The parametric fit of the experimental levels was performed by means of the program Reel (*14*) on the complete 364 * 364 basis of the f^3 configuration. The crystal field interaction has been modified by dividing the $\langle {}^2H(2) /\!/ U^4 /\!/ {}^2H(2) \rangle$ matrix element by 4 in order to improve the calculated/experimental agreement for the $^2H(2)_{11/2}$ level as is discussed in reference (*15*). The refinement was carried out by adjusting 14 free ion and 4 crystal field parameters. The process was started with the free ion values adjusted for NdF_3 (*13*). Starting values of the neodymium 4*f* electron crystal field parameters were obtained by application of a covalent model and utilizing recent observations concerning the influence of second neighbors (*16*). The crystal field at the rare earth site is produced by its ligands but the field strength and its decrease when the ligand distance increases are tuned by the next nearest neighbors. To that respect, aluminum is the element which has the most drastic influence on the order 6 parameters. We therefore utilized the method which proved efficient for $NdAlO_3$, and more generally for all mixed oxides containing neodymium and aluminium. The predicted parameters resulting from the calculation are listed in Table VII, second column. The a priori calculation takes into account the 12 oxygen first neighbors of the regular 2*d* site in the MP structure. The point symmetry around Nd therefore is D_{3h} and the Nd–O distances are deduced from the crystallographic data in Table II.

The first refinements were made on 92

experimental levels without $^4F_{3/2}$. The calculated splitting for this last transition, 70 cm^{-1}, was in good agreement with the observed difference between 11,596 and 11,662 cm^{-1}. These two lines were then taken into account. The best fit parameters on the 94 experimental values are gathered in Table VII, the root mean square deviation being 12.5 cm^{-1}. The calculated levels are reported in Table VI. For levels higher than the $^4D_{1/2}$, not all the calculated sublevels are listed, but only the nearest to the observed lines. Therefore the Nd^{3+} optical spectrum in $Ca_{0.8}Nd_{0.2}$ is well reproduced, assuming a D_{3h} point symmetry; this confirms that neodymium ions are localized on a single site very close to the regular large cation site of the MP structure. Moreover the fitted B_q^k are actually very close to the a priori calculated values, the only marked difference being $B^4_{0\text{exp}} = 2.1\ B^4_{0\text{calc}}$ (Table VII).

A similar analysis was realized on $Ca_{0.5}Nd_{0.5}$, taking into account only the absorption lines corresponding to the main site. The positions of most of the energy levels remain very close to those observed for $Ca_{0.8}Nd_{0.2}$ and should not lead to a great variation of the parameters set. The $^4I_{9/2} \rightarrow {}^4F_{3/2}$ transition is once more difficult to reproduce. It presents two broad bands centered at 11,574 and 11,696 cm^{-1} (Fig. 4b). This 122 cm^{-1} splitting would be correctly reproduced with a B_0^2 value of about 800 cm^{-1} but this value is too high to fit the other levels. From the broadness of the two lines we deduce that they are the envelopes of several narrower components and estimate the smallest possible separation between two individual lines (one of each band) to 100 cm^{-1}. The mean deviation is 14.2 cm^{-1} and the corresponding parameters are gathered in Table VII. It must also be pointed out that other terms, such as spin-correlated crystal field interactions (*17*), lead to a selective shift of some energy levels when they are included in the Hamiltonian of the system. One may infer that the $^4F_{3/2}$ Stark levels are not well fitted here because such interactions are not taken into account.

The increase of the mean deviation value with the neodymium concentration seems to arise from a limitation of the isolated ion model at high neodymium concentrations. The existence of some satellite lines on the ESR spectra at high neodymium concentrations indicates that some Nd^{3+} ion pairing occurs. In terms of the crystal field effect (or in other words of the Nd environment) ion pairing will result in differences in the second neighbors of a given Nd: either a second Nd or a Ca. Indirectly this may also cause slight distortions in the oxygen first neighbors or differences in the localization of the charge-compensating magnesium ions. Such second neighbors effects are often suggested to explain the appearance of satellite lines in the lanthanide optical spectra (*18*). In the case considered here one must admit that the structural changes affect the $^4F_{3/2}$ splitting (which depends only on B_q^2 parameters) more than the decomposition of the other levels. So besides the apparition of a second site (characterized by a lower $^2P_{1/2}$, around 23,326 cm^{-1}, and sets of lines shifted toward lower energies in the other transitions), one must also consider the broadening or the decomposition of the lines corresponding to the main site. In these conditions fitting the observed spectra for a more heavily doped sample has not been considered.

A further check of the accuracy of the crystal field parameters can be obtained from a comparison with the ESR results. The g values for the ground state Kramers doublet of Nd^{3+} have been calculated utilizing the wave vectors computed from the crystal field parameters listed in Table VII. The calculated values are in fairly good agreement with the experimental ones (for example, for $x = 0.5$ $g_{\perp\text{calc}} = 1.50$ and $g_{\perp\text{exp}} = 1.60$, $g_{/\!/\text{calc}} = 4.09$ and $g_{/\!/\text{exp}} = 3.91$).

For a given temperature, the theoretical values of the magnetic susceptibility can

TABLE VI

OBSERVED AND COMPUTED Nd^{3+} ENERGY LEVELS FOR $Ca_{0.8}Nd_{0.2}$

Levels	E_{exp} (cm^{-1})	E_{cal} (cm^{-1})	Levels	E_{exp} (cm^{-1})	E_{cal} (cm^{-1})
$^4I_{9/2}$	0	0			17,558
	150	134		19,131	19,116
	180	187		19,190	19,186
	480	484		19,271	19,279
	540	545		19,335	19,331
$^4I_{11/2}$	2,081	2,071	$^2K_{13/2}{}^4G_{9/2}$	19,512	19,520
	2,082	2,076		19,629	19,654
	2,182	2,175		19,666	19,660
		2,218		19,686	19,691
	2,262	2,251			19,737
	2,291	2,286		19,774	19,752
				19,801	19,804
$^4I_{13/2}$	4,003	4,001		19,802	19,805
	4,118	4,125			19,863
	4,161	4,162			19,918
	4,220	4,214		19,891	19,919
	4,278	4,267			19,939
	4,391	4,390			
			$^2G(1)_{9/2}{}^2D(1)_{3/2}$	21,163	21,168
$^4I_{15/2}$	5,819	5,834		21,164	21,171
	5,995	6,015		21,186	21,194
	6,107	6,117			21,353
	6,276	6,276		21,272	21,259
	6,277	6,303		21,306	21,330
	6,339	6,353		21,383	21,377
	6,596	6,609			
		6,731	$^4G_{11/2}{}^2K_{15/2}$	21,617	21,631
				21,668	21,655
$^4F_{3/2}$	11,596	11,582		21,682	21,673
	11,662	11,652			21,714
	11,685				21,738
				21,779	21,768
$^4F_{5/2}{}^2H(2)_{9/2}$	12,610	12,627		21,834	21,818
	12,633	12,631		21,881	21,878
	12,634	12,646		21,882	21,882
	12,664	12,675			21,920
	12,714	12,711			21,924
		12,861		21,954	21,955
	12,856	12,870			21,989
	12,980	13,007		21,990	22,013
$^4F_{7/2}{}^4S_{3/2}$	13,535	13,546	$^2P_{1/2}$	23,447	23,443
	13,568	13,572			
	13,717	13,731	$^2D(1)_{5/2}$	23,941	23,950
	13,744	13,744		24,015	23,999
	13,745	13,752			24,105
	13,774	13,779			
			$^2P_{3/2}$	26,340	26,342
$^4F_{9/2}$	14,863	14,876			26,430
	14,901	14,908			
	14,932	14,947	$^4D_{3/2}$	28,217	28,227

TABLE VI—*Continued*

Levels	E_{exp} (cm^{-1})	E_{cal} (cm^{-1})	Levels	E_{exp} (cm^{-1})	E_{cal} (cm^{-1})
	14,959	14,964			28,292
	15,015	14,984			
			$^4D_{5/2}$	28,369	28,359
$^2H(2)_{11/2}$	16,045	16,031		28,450	28,441
	16,084	16,067			28,541
	16,085	16,091			
	16,103	16,101	$^4D_{1/2}$	28,868	28,879
	16,118	16,113			
		16,185	$^2I_{11/2}$	29,455	29,437
$^4G_{5/2}{}^4G_{7/2}{}^2G(1)_{7/2}$	17,271	17,292	$^2L_{15/2}$	30,414	30,412
	17,310	17,332			
	17,340	17,351	$^4D_{7/2}$	30,628	30,637
	17,490	17,484			
	17,559	17,550	$^2D(2)_{3/2}$	33,501	33,501
	17,560	17,557			33,593

also be calculated utilizing the same wave vectors. For the two compounds $Ca_{1-x}Nd_x$ studied, $1/\chi_\perp$ is always higher than $1/\chi_{/\!/}$. At 300 K, the values for $x = 0.2$ and $x = 0.5$ are, respectively (in $emucgs^{-1}$), $1/\chi_{/\!/} = 182.93$, $1/\chi_\perp = 218.03$ and $1/\chi_{/\!/} = 177.78$; $1/\chi_\perp = 221.66$.

Fluorescence of Nd^{3+} in the CLnA

Fluorescence Spectra

The fluorescence of the C*Ln*A crystals in the near infrared range was performed using a Jobin–Yvon HR 1000 monochromator and a PbS cell detector associated with a lock-in amplifier. The excitation wavelength at 577 nm, in the hypersensitive absorption band, was obtained using a filtered mercury arc lamp. The only fluorescent level is $^4F_{3/2}$. The terminating level of the main emission, at about 1.06 μm, is $^4I_{11/2}$. Other transitions toward $^4I_{9/2}$ and $^4I_{13/2}$ occur at about 0.9 and 1.35 μm, respectively. They are weaker than the previous one and will not be further considered in this study. At liquid nitrogen temperature, the lowest Stark level of $^4F_{3/2}$ is the most populated. The $^4F_{3/2} \rightarrow {}^4I_{11/2}$ transition therefore consists of six strong lines. Experimentally, one observes only three bands. The emission spectra can be compared to that of LNA (Fig. 5). The maxima of the three bands are shifted toward higher energies when the calcium con-

TABLE VII

FREE ION AND CRYSTAL FIELD PARAMETERS FOR Nd^{3+} AT 4 K IN $Ca_{0.8}Nd_{0.2}$ AND $Ca_{0.5}Nd_{0.5}$

Parameters	A priori determination	$Ca_{0.8}Nd_{0.2}$ values (cm^{-1})	$Ca_{0.5}Nd_{0.5}$ values (cm^{-1})
E^0		12,340	12,355
E^1		4,828	4,818
E^2		23.8	23.8
E^3		486	487
ζ		881	880
α		20.8	20.8
β		−582	−582
γ		1,443	1,443
T^2		311	309
T^3		43	42
T^4		94	103
T^6		−264	−260
T^7		321	309
T^8		265	261
B_0^2	474	472	609
B_0^4	206	433	454
B_0^6	−1687	−1,754	−1,752
B_6^6	992	980	969
Mean deviation (cm^{-1})		12.5 (for 94 levels)	14.2 (for 72 levels)

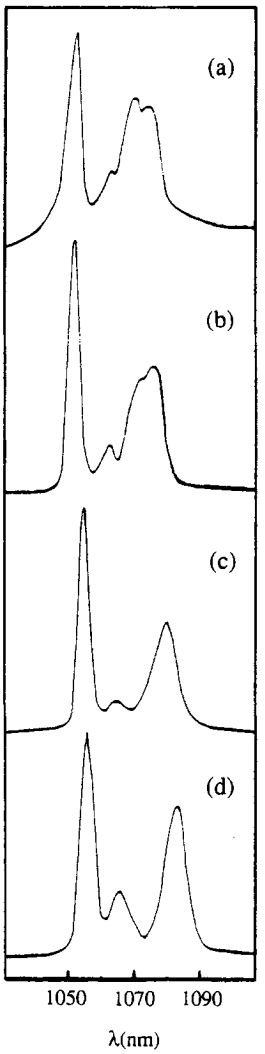

FIG. 5. Comparison of the fluorescence spectra of the Nd^{3+} $^4F_{3/2} \rightarrow {}^4I_{11/2}$ transition at 100 K. Starting compositions: (a) $Ca_{0.9}Nd_{0.1}$; (b) $Ca_{0.8}Nd_{0.2}$; (c) $Ca_{0.5}Nd_{0.5}$; and (d) LNA.

centration increases (Table VIII). One can notice also that, for the $Ca_{1-x}Nd_x$ samples with $x \leq 0.5$, the third band is split into two broad ones. The LNA values (*3*) (also reported in Table VIII) are close to those of the samples with the lowest calcium concentration. Table VIII indicates also that the crystal field variation which produces the bandshifts is mainly due to the variation of the calcium content rather than to that of neodymium. Two examples which support this assertion are given. For example, $Ca_{0.8}La_{0.1}Nd_{0.1}$ can be better compared to $Ca_{0.8}Nd_{0.2}$ than to $Ca_{0.9}Nd_{0.1}$.

Fluorescence Intensities and Lifetimes

The fluorescence lifetimes and intensity measurements were performed using a Molectron DL-12 multicell tunable dye laser pumped with a Molectron UV-14 nitrogen laser. A S1 photomultiplier detector coupled with a Tektronix 2430 A digital oscilloscope is used to collect and analyze the fluorescence.

It is interesting to estimate the concentration dependence of the Nd^{3+} fluorescence intensity. On geometrically identical $Ca_{1-x}Nd_x$ samples, the variation of the fluorescence maximum intensity I_0, just at the beginning of the fluorescence decay, shows a maximum around $x = 0.35$. This value is higher than for LNA ($La_{1-x}Nd_xMgAl_{11}O_{19}$). A previous study performed on polycrystalline LNA samples with various Nd^{3+} concentrations has shown a maximum value of the fluorescence intensity for approximately $x = 0.15$ (*19*).

TABLE VIII

MAXIMA OBSERVED FOR THE $^4F_{3/2} \rightarrow {}^4I_{11/2}$ FLUORESCENCE OF Nd^{3+} AT 100 K FOR DIFFERENT C*Ln*A COMPOUNDS AND LNA

Initial compositions	First band (nm)	Second band (nm)	Third band (nm)	
LNA[a]	1055.6	1065.8	—	1082.8
$Ca_{0.3}Nd_{0.7}$	1054.8	1065	—	1080.2
$Ca_{0.4}Nd_{0.6}$	1054.2	1064.8	—	1079.3
$Ca_{0.5}Nd_{0.5}$	1053.6	1063.4	—	1078.6
$Ca_{0.5}La_{0.4}Nd_{0.1}$	1054.0	1063.6	—	1078.4
$Ca_{0.6}Nd_{0.4}$	1053.4	1062.8	1074.4	1077.2
$Ca_{0.7}Nd_{0.3}$	1053.2	1062.6	1073.2	1077
$Ca_{0.8}Nd_{0.2}$	1051.2	1062.4	1071.6	1075
$Ca_{0.8}La_{0.1}Nd_{0.1}$	1052.0	1063.4	1071.2	1075.2
$Ca_{0.9}Nd_{0.1}$	1050	1061	1068.8	1073.2

[a] Values measured for the composition $La_{0.9}Nd_{0.1}MgAl_{11}O_{19}$.

TABLE IX

FLUORESCENCE LIFETIMES FOR VARIOUS Nd^{3+} RATES IN THE $Ca_{1-x}Nd_x$ COMPOUNDS

X (Nd^{3+} rate)	$N_{Nd^{3+}}$ (10^{20} atoms/cm^3)	Lifetimes (μsec)
0.139	4.74	170
0.254	8.65	54
0.491	16.71	22
0.581	19.76	11
0.608	20.61	17

Table IX reports the values of the fluorescence lifetimes for Nd^{3+} compositions between 5×10^{20} and 2×10^{21} Nd^{3+} ions/cm^3. For identical neodymium concentrations, LNA presents approximately the same lifetime values. Since the decay curves are nonexponential, a mean lifetime value τ_m is defined by the equation $\tau_m = 1/I_0 \int_0^\theta I(t)dt$, where I_0 is the fluorescence intensity at $t = 0$ and θ the time at which the fluorescence intensity drops below the dark current value of the detector. It is important to notice that a strong decrease of the fluorescence lifetime occurs when the concentration increases. This behavior is characteristic of a strong concentration quenching by the cross-relaxation process (*20*), well known in Nd^{3+} activated hosts.

At last, one can notice that the Nd^{3+} decay rate is very short when the maximum of the fluorescence intensity is reached. Concerning a potential interest in these materials as lasers, a compromise between the fluorescence intensity and the decay rate would have to be chosen.

Discussion and Conclusion

Our study establishes that $Ca_{1-x}Nd_x$ crystals can be synthesized by the floating zone method in the range $0.1 \leq x \leq 0.7$. For the compositions with a very high calcium rate, the melting becomes noncongruent.

In order to maintain a low rate of neodymium and to avoid quenching of fluorescence, while preventing the formation of parasitic phases, one can introduce lanthanum ions to decrease the calcium content. On the other hand, it has been shown that the structural and crystal-field-dependent optical properties are determined by the calcium rate of the compounds. For $x \leq 0.2$, the Nd^{3+} ions seem to be localized only in the regular large cation site of the MP structure with D_{3h} symmetry. The structural and optical absorption investigations corroborate the fact that the presence of calcium decreases most of the distortions of the MP structure, which are usually observed for lanthanide hexaaluminates (*21*).

Let us compare these results with those obtained in a previous study of LNA (*8*). In this compound, it has been shown that the energy levels found experimentally cannot be fitted with a single set of free ion and crystal field parameters. At least two sets, differing mainly in the free ions values, were necessary: one to fit the low energy lines of the 4 K absorption spectrum and the other for the high energy ones. This conclusion is in good accordance in particular with the detection at 4 K of essentially two $^4I_{9/2} \rightarrow {}^2P_{1/2}$ absorption lines (if one neglects the splitting of the high energy doublet). These two lines appear at 426.4 and 429.7 nm, respectively, in LNA (Fig. 3c). For $Ca_{0.8}Nd_{0.2}$ only one line at 426.6 nm is seen and the crystallographic analysis concludes at one single site for Nd^{3+} at $6h$ with $x = 0.6736$ very near from the $2d$ ($x = 0.6667$) position. Actually the absorption spectrum is well fitted with the D_{3h} symmetry (Nd in the MP regular $2d$ site) and there is a good correlation between the a priori calculation of the B_q^k's for this site and those experimentally determined.

We will now discuss the "low energy" site in $Ca_{0.5}Nd_{0.5}$ which is responsible for the apparition of a 428.7-nm (23,326 cm^{-1}) weak line beside the 426.6-nm (23,447 cm^{-1}) main component (Fig. 3b) in the $^4I_{9/2} \rightarrow {}^2P_{1/2}$ tran-

sition. May this line be attributed to the second site deduced from the structure refinement ($6h$ localization with $x = 0.6855$)? The prediction of the crystal field parameters has been made following the same principles as those above (cf. the preceding paragraph) for three situations: Nd^{3+} in $6h$, $x = 0.6736$ (the case of $Ca_{0.8}Nd_{0.2}$, Table III), in $2d$, $x = 0.6667$, and in $6h$, $x = 0.6855$, the two sites deduced from diffraction data in $Ca_{0.5}Nd_{0.5}$ (Table IV). The level energies calculated a priori for these three cases may then be compared, assuming that the free ion parameters do not change. The true D_{3h} point site and that of the slightly distorted C_{2v} ($x = 0.6736$) actually give very similar calculated spectra. The mean deviation of this slightly distorted C_{2v} site calculated with respect to D_{3h} on 98 levels up to $^2P_{1/2}$ is 12 cm^{-1}, whereas it is 25 cm^{-1} for the strongly distorted C_{2v} site ($x = 0.6855$) compared to D_{3h}. In other words, the calculated energy scheme for $x = 0.6855$ is too different from D_{3h} to suppose that the two spectra overlap in the observed linewidths. It is then very probable that the two point sites deduced from X-ray diffraction data in $Ca_{0.5}Nd_{0.5}$ actually give rise to the two absorption spectra observed. The first one is very preponderant for neodymium and very near the D_{3h} symmetry, and gives almost the same spectrum as $Ca_{0.8}Nd_{0.2}$. The second site, very distorted with respect to the ideal MP one, is very poorly occupied by neodymium in $Ca_{0.5}Nd_{0.5}$ but its occupation becomes more important as the calcium content is lowered to LNA.

The position of the weak $^4I_{9/2} \rightarrow {}^2P_{1/2}$ line at a wavelength higher than the strongest component is in agreement with the preceding description. Studies by Caro and Derouet (*22*) have shown that there is a correlation between the 4 K $^4I_{9/2} \rightarrow {}^2P_{1/2}$ line and the coordination of Nd^{3+} in ionic matrices. Indeed the line around 426.6 nm is at the wavelength expected for 12-fold coordination (as in $LaAlO_3:Nd^{3+}$ (*22*)), while Nd^{3+} in YAG (*22*) or in $Ca_2Ga_2SiO_7$ (*23*), both exhibiting height-fold coordination, has $^2P_{1/2}$ lines near 430 nm. This is exactly the domain where the "high wavelength" line of LNA and the second line of $Ca_{0.5}Nd_{0.5}$ occur. Actually the coordination around Nd^{3+} ($6h$) diminishes when the distortion increases (see Table V). At stronger shifts from the regular ($2d$) site, the coordination may even be 8 as has been detected in several lanthanide magnetoplumbites (*7*). We must also pay attention to the influence of the magnesium which balances the introduction of Ln^{3+} ions, prevents the creation of vacancies in the unit cell, and then stabilizes the structure.

The ESR study shows the occurrence of interactions between Nd^{3+} ions for high neodymium content. This ion pairing could be related to the problem of the supplementary lines and high splitting of the $^4I_{9/2} \rightarrow {}^4F_{3/2}$ transition and to the strong decrease of the fluorescence lifetime when the neodymium concentration increases. However, the question of the increase of the fluorescence intensity, while strong cross-relaxation between Nd^{3+} ions occurs, remains to be answered. These results prompt us to undertake a detailed ESR investigation in order to understand the origin and behavior of these ion–ion interactions.

The aim of our work is to consider whether the C*Ln*A could be a laser material. Obviously, the fast decrease of the Nd^{3+} decay rate and its low value at the fluorescence intensity of a practical usefulness maximum should limit the range of the x values for laser applications. However, we note the potential tunability of the laser emission associated with the broadness of the lines. If one considers the high wavelength group of lines of the fluorescence spectra depicted in Fig. 5, one can expect tunability from 1062 to 1074 nm for the compounds with high calcium content which give the broadest lines, assuming that it would extend over the linewidth at half height.

One of the interests of the C*Ln*A compounds as a laser matrix is also in the possibility offered by their structure to accommodate different ions as coactivators. The potential of LMA : Nd^{3+} containing Cr^{3+} ions is now well established (*24, 25*). Energy transfer occurs between Cr^{3+} and Nd^{3+}. It allows an increase in the laser slope efficiency while decreasing the thermal lensing problem. Such energy transfers are under study with the $Ca_{1-x}Nd_x$ compounds.

The $LnMgAl_{11}O_{19}$ compounds exist for all the large Ln^{3+} ions (from La to Gd); a few experiments have been made in order to determine whether the C*Ln*A phase also forms for other Ln^{3+} ions besides Nd^{3+}. A few attempts were made to incorporate Pr^{3+}. Single crystals of $Ca_{1-x}Pr_x$ compounds can be grown by the floating zone method with results very similar to those already reported for Nd^{3+}. It has been shown previously (*8*) that in $PrMgAl_{11}O_{19}$, Pr^{3+} ions are distributed among at least two different sites. This was demonstrated by the number of lines for the $^3H_4 \rightarrow {}^3P_0$ absorption transition of Pr^{3+} at 4 K. Preliminary studies made with the $Ca_{1-x}Pr_x$ phases in a similar way indicate that the Pr^{3+} ions tend to occupy a single site when the calcium content of the compound increases.

Further studies on these materials and attempts to grow single crystals by the Czochralski method in order to obtain large samples, on which laser tests could be made, will be performed in the near future.

Acknowledgments

The authors are indebted to L. Trouilleux, G. Dhalenne, and A. Revcolevschi (Laboratoire des Composés Non Stoechiométriques, Université Paris-Sud, Orsay, France) for their help in crystal growth by the floating zone method. The authors thank J. C. Daran and F. Robert for careful x-ray data collection on single crystals. The authors also thank D. Simons and P. Aschehoug for their technical assistance, respectively, in the ESR and fluorescence investigations. The work was supported in part by the Quartz et Silice Company.

References

1. T. Gbehi, J. Thery, D. Vivien, R. Collongues, G. Dhalenne, and A. Revcolevschi, *J. Solid State Chem.* **77,** 211 (1988).
2. D. Vivien, A. M. Lejus, J. Thery, R. Collongues, J. J. Aubert, R. Moncorge, and F. Auzel, *C.R. Acad. Sci.* **298**(2), 195 (1984).
3. L. D. Schearer, M. Leduc, D. Vivien, A. M. Lejus, and J. Thery, *IEEE J. Quantum Electron.* **22,** 713 (1986).
4. A. Utsunomiya, K. Tanakawa, F. Marumo, and H. Kojima, *J. Solid State Chem.* **75,** 197 (1988).
5. W. R. Busing, K. O. Martin, and H. A. Levy, "UAX Adaptation of OXFLS-Routine," Oakridge National Laboratory Press, Oakridge, TN (1972).
6. "International Tables for X-Ray Crystallography," Vol. IV, Kynoch Press, Birmingham, England (1974).
7. M. Gasperin, M. C. Saine, A. Kahn, F. Laville, and A. M. Lejus, *J. Solid State Chem.* **54,** 61 (1984).
8. D. Saber, J. Dexpert-Ghys, P. Caro, A. M. Lejus, and D. Vivien, *J. Chem. Phys.* **82,** 5648 (1985).
9. B. Bleaney, R. J. Elliott, and H. E. D. Scovil, *Proc. Phys. Soc. A* **64,** 933 (1951).
10. N. I. Agladze, V. A. Antonov, P. A. Arsen'ev, Kh. S. Bagdasarov, V. F. Zolin, V. M. Markushev, I. T. Makhmudov, and M. N. Popova, *Zh. Prikl. Spektrosk.* **43,** 798 (1985).
11. E. Antic-Fidancev, M. Lemaitre-Blaise, L. Beaury, T. de Sagey, and P. Caro, *J. Chem. Phys.* **73,** 4613 (1980).
12. P. Caro, J. Derouet, L. Beaury, and E. Soulie, *J. Chem. Phys.* **70,** 2542 (1979).
13. P. Caro, J. Derouet, L. Beaury, T. de Sagey, J. P. Chaminade, J. Aride, and M. Pouchard, *J. Chem. Phys.* **74,** 2698 (1981).
14. P. Porcher, "Phenomenological Treatment of Rare Earth Configurations: Routines REEL and IMAGE," unpublished.
15. M. Faucher, D. Garcia, and P. Porcher, *C.R. Acad. Sci.* **308,** 603 (1989).
16. M. Faucher, D. Garcia, and O. K. Moune, submitted for publication.
17. C. K. Jayasankar, M. F. Reid, and F. S. Richardson, *Phys. Status Solidi* **155,** 559 (1989).
18. R. Buisson, J. Q. Liu, and J. C. Vial, *J. Phys.* **45,** 1533 (1984).
19. A. Kahn, A. M. Lejus, M. Madsac, J. Thery, D. Vivien, and J. C. Bernier, *J. Appl. Phys.* **52,** 6864 (1981).
20. F. Auzel, *Mater. Res. Bull.* **14,** 223 (1979).

21. R. COLLONGUES, D. GOURIER, A. KAHN-HARARI, A. M. LEJUS, J. THERY, AND D. VIVIEN, *Annu. Rev. Mater. Sci.* **20,** 51 (1990).
22. P. CARO AND J. DEROUET, *Bull. Soc. Chim. Fr.* **1,** 46 (1972).
23. A. A. KAMINSKII, E. L. BELOKONEVA, B. V. MILL, S. E. SARKISOV, AND K. KURBANOV, *Phys. Status Solidi* **97,** 279 (1986).
24. C. G. AMINOFF, C. LARAT, M. LEDUC, B. VIANA, AND D. VIVIEN, *J. of Lumin.* **50,** 21 (1991).
25. B. VIANA, C. GARAPON, A. M. LEJUS, AND D. VIVIEN, *J. of Lumin.* **47,** 73 (1990).